Journal of Power Sources 195 (2010) 969–976

Contents lists available at ScienceDirect

Journal of Power Sources

journal homepage: www.elsevier.com/locate/jpowsour

Electrical properties of ceria Co-doped with Sm^{3+} and Nd^{3+}

Bin Li, Yanyi Liu, Xi Wei, Wei Pan*

State Key Lab. of New Ceramics and Fine Processing, Department of Materials Science and Engineering, Tsinghua University, Beijing 100084, People's Republic of China

ARTICLE INFO

Article history:
Received 27 July 2009
Received in revised form 31 August 2009
Accepted 1 September 2009
Available online 6 September 2009

Keywords:
Co-doping
Ceria
Solid oxide fuel cells
Activation energy
Segregation

ABSTRACT

Ceria co-doped with Sm^{3+} and Nd^{3+} powders are successfully synthesized by citric acid–nitrate low-temperature combustion process. In order to optimize the electrical properties of the series of ceria co-doped with Sm^{3+} and Nd^{3+}, the effects of co-doping, doping content and sintering conditions on grain and grain boundary conductivity are investigated in detail. For the series of $Ce_{0.9}(Sm_xNd_{1-x})_{0.1}O_{1.95}$ (x = 0, 0.5, 1) and $Ce_{1-x}(Sm_{0.5}Nd_{0.5})_xO_\delta$ (x = 0.05, 0.10, 0.15, 0.20) sintered under the same condition, $Ce_{0.9}(Sm_{0.5}Nd_{0.5})_{0.1}O_{1.95}$ exhibits both higher grain and grain boundary conductivity. Compared with $Ce_{0.9}Gd_{0.1}O_{1.95}$ and $Ce_{0.8}Sm_{0.2}O_{1.9}$, $Ce_{0.9}(Sm_{0.5}Nd_{0.5})_{0.1}O_{1.95}$ sintered at 1350–1400 °C shows higher total conductivity with the value of 1.0×10^{-2} S cm^{-1} at 550 °C. In addition, it can be found the trends of grain and grain boundary activation energies of $Ce_{1-x}(Sm_{0.5}Nd_{0.5})_xO_\delta$ are both consistent with those of $Ce_{1-x}Nd_xO_\delta$, but different from those of $Ce_{1-x}Sm_xO_\delta$, which can be explained as: the local ordering of oxygen vacancies maybe occurs more easily in Nd-doped ceria than in Sm-doped ceria; the segregation amount of Sm^{3+} is more than that of Nd^{3+} to the grain boundaries in ceria co-doped with Sm^{3+} and Nd^{3+}, which is confirmed by X-ray photoelectron spectroscopy (XPS).

1. Introduction

Recently, solid oxide fuel cells (SOFCs) are of considerable interest as efficient and clean energy convertors. The performance of the oxide-ion electrolyte of the SOFC is critical to the development of a low or intermediate-temperature system. Although yttria-stabilized zirconia (YSZ) electrolyte has been used in SOFC under commercial development, their operating temperature are too high (800–1000 °C), which leads to high costs of interconnector and other construction materials, as well as short lifetimes of the devices [1–3]. Therefore, there remains a strong motivation to search for new, improved oxide-ion electrolytes. Especially, doped ceria electrolytes are being investigated in view of its immense potential for the development of low-temperature solid electrolytes. In the family of doped ceria electrolytes, Gd-doped or Sm-doped ceria were recognized to have higher ionic conductivity [1–3]. Many strategies have been adopted to improve the properties of such oxides further by co-doping techniques [4–7] or by using alternate processing techniques [4,8,9].

Co-doping technique has been widely accepted to be an effective method to enhance the grain conductivity of ceria-based electrolytes. Generally, the conductivity σ is temperature dependent, and it can be expressed by the well-known Arrhenius relationship,

$$\sigma T = \sigma_0 \exp\left(-\frac{E_a}{kT}\right) = \sigma_0 \exp\left(-\frac{\Delta H_m + \Delta H_a}{kT}\right) \quad (1)$$

where T denotes the temperature, and σ_0 is the pre-exponential factor being a constant in a certain temperature range, and E_a represents the activation energy which is the sum of the migration enthalpy (ΔH_m) and the association enthalpy (ΔH_a), and k is Boltzmann constant. According to Eq. (1), the choice of dopants is based on minimizing the activation energy of oxygen diffusion. According to Kilner and Brook [10], association enthalpy is minimal when there is no elastic strain present in the host lattice. Based on that, Kim explained the reason why the doping of Gd is effective in ceria is that the dopant has an "optimum radius" (0.104 nm) for the trivalent cation, which causes no expansion nor contraction in the ceria lattice [11]. Omar et al. [5] tried to improve the ionic conductivity by simultaneously adding Nd and Lu into ceria for matching "optimum radius". However, the electrical property of ceria co-doped with Nd and Lu is poorer than that of ceria doped with Gd, which shows it is not enough only to consider the elastic energy. Recently, Andersson et al. [12] proposed the balance of repulsive elastic and attractive electronic parts for the association energy of dopant-vacancy clusters, which maybe offers a simple and clear way to narrow the search for superior dopants and combinations of dopants. By density function theory, the ideal dopant was estimated to have an effective atomic number between 61 (Pm) and 62 (Sm) for the lowest activation energy. Unfortunately, because Pm is radioactive, it is inconceivable to use it in real

* Corresponding author. Tel.: +86 10 62772858; fax: +86 10 62771160.
E-mail addresses: bli05@mails.tsinghua.edu.cn (B. Li), panw@mail.tsinghua.edu.cn (W. Pan).

0378-7753/$ – see front matter © 2009 Elsevier B.V. All rights reserved.
doi:10.1016/j.jpowsour.2009.09.001

Table 1
Compositions, grain sizes of the powders, and densities for ceria co-doped with Sm^{3+} and Nd^{3+}.

Composition		Grain size (nm)	Actual density (g cm^{-3})	Theoretical density (g cm^{-3})	Relative density (%)
$Ce_{0.9}(Sm_xNd_{1-x})_{0.1}O_{1.95}$	$x=0$	6.0	6.68	7.12	93.8
	$x=0.5$	6.0	6.78	7.15	94.8
	$x=1$	6.2	6.80	7.18	94.7
$Ce_{1-x}(Sm_{0.5}Nd_{0.5})_xO_\delta$	$x=0.05$	5.6	6.79	7.19	94.4
	$x=0.10$	6.0	6.78	7.15	94.8
	$x=0.15$	5.8	6.69	7.12	94.0
	$x=0.20$	5.5	6.65	7.09	93.8

application. As proposed by Andersson et al., a mixture of dopants added into ceria, such as Nd and Sm, may result in the enhancement of ionic conductivity, which is confirmed by the experiments of our group [13] and Omar et al. [14]. As reported by Omar et al. [14], the ceria co-doped with Sm and Nd were synthesized by solid-state reactions. The samples were sintered at high temperature of 1550 °C for 10 h in order to achieve high relative density. Among the series, $Ce_{0.9}Sm_{0.05}Nd_{0.05}O_{1.95}$ shows the highest grain conductivity, which is higher than that of $Ce_{0.9}Gd_{0.1}O_{1.95}$. However, the composition with highest total conductivity cannot be obtained, because the grain boundary conductivity is relative to the doping content [15–20] For example, it has been found by Zhan et al. [16] and Pérez-Coll et al. [17] that $Ce_{0.9}Sm_{0.1}O_{1.95}$ exhibits higher grain conductivity but much lower grain boundary conductivity than $Ce_{0.9}Sm_{0.2}O_{1.9}$, which limits its application to SOFC. In order to lower the operating temperature, it is necessary to reduce the grain boundary resistivity. This is ascribed to the higher activation energy of the grain boundary conductivity than that in the grain [9,21].

In addition, proper sintering condition needs to be optimized for ceria co-doped with Sm^{3+} and Nd^{3+}, because it is a critical factor to influence grain boundary conductivity. It is known that dense ceria-based materials are obtained very difficultly at lower temperature and for shorter sintering time by the conventional solid-state reaction method [15]. As investigated by many researchers, the grain boundary conductivity can be largely reduced for the samples sintered at higher temperatures [22–24]. The nanosized surface-active ceramic powders have been proved to be one of the most effective routes to decrease the sintering temperature and time. In order to improve the sinterability, the method of citric acid–nitrate low-temperature combustion process can be taken into account [8,20]. Besides, compared with conventional solid-state reaction method, the above method can make different metal ions mixed more homogeneously by the chelation of citric acid, which has great effect on the improvement of the electrical properties.

In the present work, the composition and sintering conditions corresponding to highest total conductivity are obtained, and the effects of co-doping, doping content, and sintering conditions on grain and grain boundary conductivity for ceria co-doped with Sm^{3+} and Nd^{3+} have been investigated in detail.

2. Experimental

Ceria co-doped with Sm^{3+} and Nd^{3+} was synthesized by citric acid–nitrate low-temperature combustion process as introduced by our previous study [22]. Analytical reagents $Ce(NO_3)_3{\cdot}6H_2O$ (≥99.9 wt%, Yutai Qingda, China), $Sm(NO_3)_3{\cdot}6H_2O$ (≥99.9wt%, Yutai Qingda, China), $Nd(NO_3)_3{\cdot}6H_2O$ (≥99.9wt%, Yutai Qingda, China), and $C_6H_8O_7{\cdot}H_2O$ (≥99.0wt%, Modern Eastern, China) were used as starting materials. The molar ratio of the metal ions to citric acid was 1:1.2. Stoichiometric amounts of $Ce(NO_3)_3{\cdot}6H_2O$, $Sm(NO_3)_3{\cdot}6H_2O$ and $Nd(NO_3)_3{\cdot}6H_2O$ were dissolved in deionized water to form transparent solution. The total concentration of metal ions was controlled to be about 0.1 mol l^{-1}. Then citric acid was added into the solution with stirring for about 1 h. The transparent solution was heated at 95 °C in a water bath until the yellow gel was yielded, and then dried in a constant temperature drying oven at 80 °C for 12 h. The dried gel was heated in the air on the electric oven and self-ignited until the yellow powders without black carbons were generated. $Ce_{0.9}(Sm_xNd_{1-x})_{0.1}O_{1.95}$ ($x=0$, 0.5 and 1) and $Ce_{1-x}(Sm_{0.5}Nd_{0.5})_xO_\delta$ ($x=0.05$, 0.10, 0.15 and 0.20) were successfully synthesized by that method. SiO_2 weight content of the powders, which was characterized by inductively coupled plasma mass spectroscopy (ICP, X Series), was all less than 50 ppm. The powders were sieved to 100 meshes, uni-axially dry-pressed into pellets (φ10 mm) under 200 MPa, and then sintered at different sintering temperatures (1300–1450 °C) for 4 h. All the specimens were sintered in air and heated by the rate of 240 °C h^{-1}, and then furnace-cooled after sintering. Densities of the sintered pellets were determined by Archimedean method.

Phase identification and analysis were conducted by X-ray diffraction (XRD). Two kinds of XRD scans were performed using an X-ray diffractometer (Rigaku, D/max-RB, Japan) with nickel-filtered Cu Kα radiation. Continuous scans (6° min^{-1}) were used for qualitative phase identification, while slow step scans at a rate of 0.02°/2 s were conducted to determine the shifts of the X-ray spectrum and the full width at half maximum of a peak. Hence, lattice parameters of the specimens were calculated from slow step

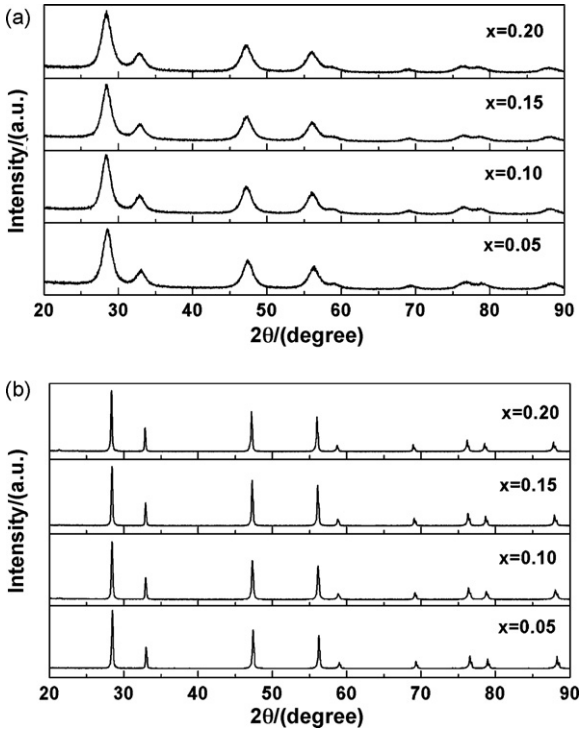

Fig. 1. XRD patterns of the powders (a) and the sintered pellets (b) of Sm^{3+} and Nd^{3+} co-doped $Ce_{1-x}(Sm_{0.5}Nd_{0.5})_xO_\delta$ with $x=0.05$, 0.10, 0.15 and 0.20.

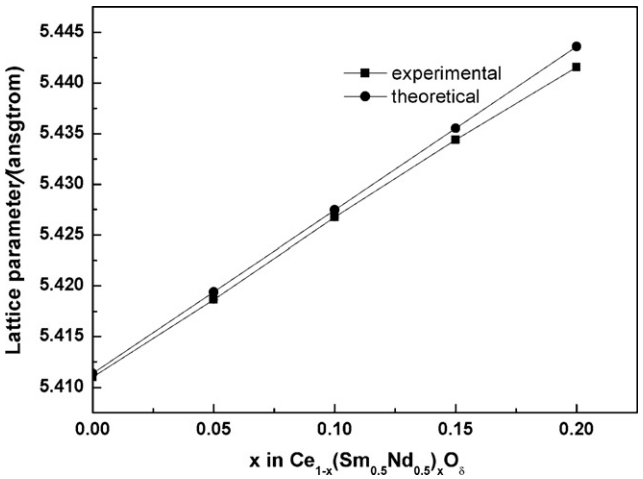

Fig. 2. Lattice parameters of the specimens (experimental and theoretical) sintered at 1400 °C for 4 h as a function of the amount of dopants.

scan XRD data, using the least-squares method. Besides, the average grain size of the powders can be estimated by Scherrer equation. The sintered pellets were polished, and thermally etched at 1350 °C for 1 h. X-ray photoelectron spectroscopy (XPS, PHI Quantera SXM) was introduced to analyze the elemental composition of surfaces qualitatively and quantitatively, which was confirmed to correspond to the elemental composition of grain boundaries, as reported by Theunissen et al. [25]. And then these samples were gold coated for microstructural analysis using field-emission scanning electron microscopy (FESEM, JSM-6301F). The average grain sizes were obtained from FESEM micrographs of the etched samples by using the linear intercept technique described by Mendelson [26]. The grain and grain boundary conductivities in air were determined by ac impedance spectroscopy (Zahner, IM6, German). Silver pastes were coated on both surfaces of the sintered pellets, and then fired at 550 °C for 30 min. Impedance measurement was performed from 150 to 700 °C with an increment of 50 °C in a frequency range from 0.1 Hz to 8 MHz with an applied voltage of 100 mV, and followed by analyzing the results using Z-View software.

3. Results and discussions

Fig. 1 shows the XRD patterns of the powders and the samples (sintered at 1400 °C for 4 h) of Sm and Nd co-doped $Ce_{1-x}(Sm_{0.5}Nd_{0.5})_xO_\delta$ with $x = 0.05$, 0.10, 0.15 and 0.20. It can be seen that only the pure ceria cubic phase is identified by XRD for all the compositions. As shown in Fig. 1(a), very wide peak shape corresponds to a small crystallite size. According to Scherrer equation, the average crystallite sizes of all the synthesized powders are nanosized and estimated to be about 5.5–6 nm, which are independent of the compositions and listed in Table 1. It is possible to obtain relatively dense bulk sintered at lower temperature. Besides, it can be observed in Fig. 1(b) that the peaks shift to smaller theta angle direction with increasing the amount of dopants, suggesting the lattice parameters should become larger with the increase of the amount of dopants. As is known, the relative density has great effect on grain boundary conduction, and the theoretical density can be calculated by measured lattice parameters. Fig. 2 shows the lattice parameters of the specimens sintered at 1400 °C for 4 h as a function of the amount of dopants. If the defect reaction could be described by the following formula:

$$xMO_{1.5} + (1-x)CeO_2 \rightarrow xM'_{Ce} + 0.5xV_{\ddot{O}} + (1-x)Ce^x_{Ce} + (2-0.5x)O^x_O \quad (2)$$

Table 2
Relative densities and grain sizes for $Ce_{0.9}(Sm_{0.5}Nd_{0.5})_{0.1}O_{1.95}$ sintered at different temperatures from 1300 to1450 °C.

	Sintering temperature (°C)			
	1300	1350	1400	1450
Relative density (%)	90.9	94.3	94.8	97.3
Grain size (μm)	0.65	0.78	0.98	2.43

as proposed by Hong and Virkar [27], the equation used for the calculation of theoretical lattice parameters for all $MO_{1.5}$–CeO_2 solid solutions is as follows:

$$a(x, r_M) = \frac{4}{\sqrt{3}}[xr_M + (1-x)r_{Ce} + (1-0.25x)r_O + 0.25xr_{V_O}] \times 0.9971 \quad (3)$$

where r_M, r_{Ce}, r_O and r_{V_o} represent the effective ion radius of doping elements, Ce, O and oxygen vacancy, respectively. For M = Sm and Nd, r_M is the average ion radius of Sm^{3+} and Nd^{3+}. As shown in Fig. 2, the lattice parameter increases linearly with increasing x following Vegard's law, due to the larger radius of Sm^{3+} (1.079 Å) or Nd^{3+} (1.109 Å) than "optimum radius" (1.04 Å) [11]. And the experimental values are consistent with the theoretical values, which can clarify the defect reaction is reasonable, and Eq. (3) can also be used in co-doping ceria system.

The theoretical density (D_{theo}) can be obtained using the following equation:

$$D_{theo} = \frac{4xM_d + 4(1-x)M_{Ce} + 4(2-0.5x)M_O}{N_A[a(x, r_M)]^3} \quad (4)$$

where M_d, M_{Ce} and M_O represent atomic mass of doping elements, Ce and O, N_A is Avagadro's number. The theoretical density, actual density and relative density are all listed in Table 1. From Table 1, it can be clearly seen that the relative density hardly changes for all the compositions sintered under the same sintering condition, which makes it convenient to discuss the grain boundary conduction below. However, the relative density increases with improving the sintering temperature from 1300 to 1450 °C, as displayed in Table 2.

Fig. 3(a)–(d) shows FESEM micrographs of the sintered $Ce_{0.9}(Sm_{0.5}Nd_{0.5})_{0.1}O_{1.95}$ at different sintering temperatures. With increasing the sintering temperature, the pores are reduced in agreement with the enhancement of relative density. In addition, the average grain size becomes larger simultaneously from 0.65 to 2.43 μm, which is listed in Table 2. For the compositions sintered under the same condition, the grain size scarcely varies, which provides a precondition that the variety of apparent grain boundary conductivity discussed below via compositions can correctly reflect that of the specific (single) grain boundary conductivity.

Different schematic equivalent circuits and corresponding ac impedance responses were shown in our previous study [22]. Generally, in polycrystalline specimens, independent semicircular arcs from high frequency to low frequency correspond to the conduction across the grains, grain boundaries, and the electrode-specimen interface, respectively. As the temperature is increased, the arcs are shifted into higher frequencies, which leads to the successive disappearance of grain and grain boundary arc. Therefore, the grain (R_g) and grain boundary (R_{gb}) resistance cannot be separated at higher measured temperature. However, as reported by Li et al. [23] and Pérez-Coll et al. [28], the grain boundary conduction shows an almost linear behavior in the Arrhenius representation. It is possible to extrapolate the grain boundary resistance data and then subtract these values from the total resistance ($R_{tol} = R_g + R_{gb}$) to estimate the grain resistance, as proposed elsewhere. In general, each individual resistance, R_i, can be formally converted to a conductivity σ_i, using

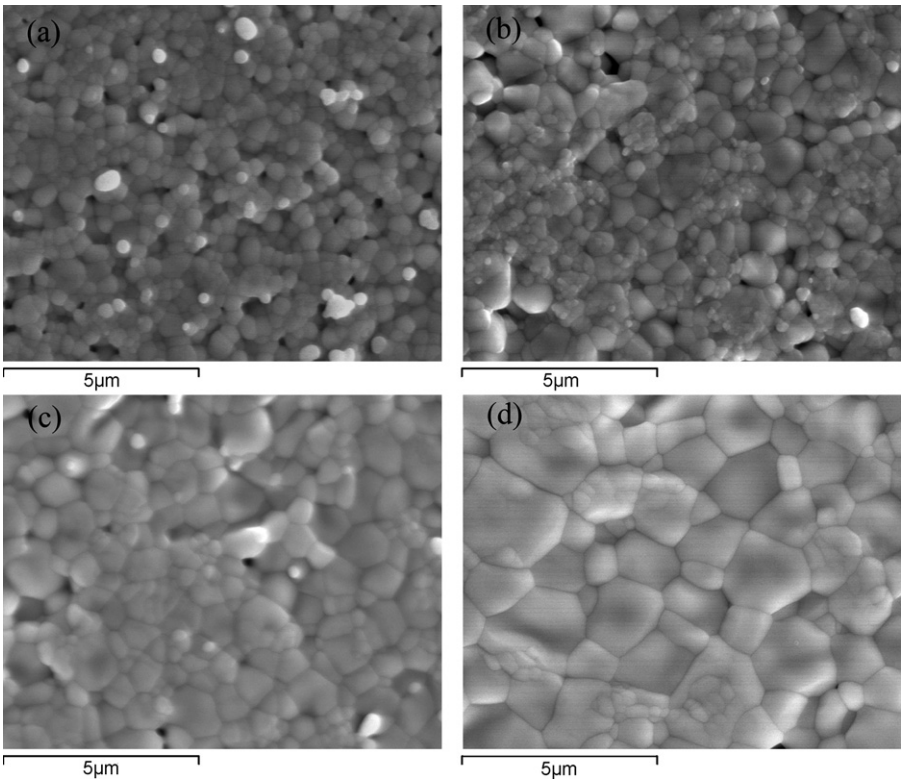

Fig. 3. FESEM micrographs of the sintered $Ce_{0.9}(Sm_{0.5}\ Nd_{0.5})_{0.1}O_{1.95}$ at different sintering temperatures. 1300 °C (a); 1350 °C (b); 1400 °C (c); 1450 °C (d).

the equation

$$\sigma_i = \frac{l}{R_i S} \tag{5}$$

where l is the sample thickness and S is the electrode area of the sample surface. In this way, the total conductivity (σ_{tol}), the grain conductivity (σ_g), and the apparent grain boundary conductivity (σ_{gb}) can be obtained.

Fig. 4 represents the grain and the grain boundary contributions and total electrical conductivity of $Ce_{0.9}(Sm_xNd_{1-x})_{0.1}O_{1.95}$ sintered at 1400 °C for 4 h with $x = 0$, 0.5 and 1. The doping level is kept to be 10 mol%. It can be observed from Fig. 4(a), ceria co-doped with Sm and Nd exhibits the highest grain conductivity, which is about 1.60×10^{-2} S cm^{-1} at 550 °C, and ceria doped with Nd exhibits the lowest conductivity. In addition, Fig. 4(a) demonstrates significant bending of the Arrhenius plots, which is usually interpreted as a transition from associated to disassociated behavior about defect clusters, that is, from a low-temperature regime, where the activation energy combines migration enthalpy (ΔH_m) and defect association enthalpy (ΔH_a), to the high temperature regime with migration enthalpy only [2,23,29]. However, there is not always a clear transition point in the curve, maybe owing to the large measured temperature increment (50 °C). As observed in Fig. 4(a), the transition temperature lie among $T = 400$–500 °C. So we calculate corresponding activation energy according to Eq. (1) in the temperature ranges of 150–400 and 500–700 °C, respectively. Fig. 5 shows the activation energies and $\ln\sigma_0$ for different compositions. It can be found that compared with Nd-doped and Sm-doped ceria, for ceria co-doped with Sm and Nd, migration enthalpy reduces, and association enthalpy increases, but the sum of them at higher temperatures changes a little, which are different from the results calculated by Andersson et al. [12]. This is maybe due to the different dopant concentration range (4.2 mol%, Andersson et al.; 10 mol%, our work). So the improvement of the grain conductivity for $Ce_{0.9}(Sm_xNd_{1-x})_{0.1}O_{1.95}$ mostly lies on the improvement of $\ln\sigma_0$, as illustrated in Fig. 5, which is due to the raise of a configurational entropy. The phenomenon that co-doping can lead to the increase of $\ln\sigma_0$ has also been found in other co-doping ceria series, and discussed by some investigators [30].

In addition, from Fig. 4(b), it is found that the sequence of grain boundary conductivity is $Ce_{0.9}(Sm_{0.5}Nd_{0.5})_{0.1}O_{1.95} \approx Ce_{0.9}Nd_{0.1}O_{1.95} > Ce_{0.9}Sm_{0.1}O_{1.95}$. Because the samples were sintered under the same condition, and the relative density changes little (Table 1), the enhancement of grain boundary conductivity primarily depends on the variety of compositions. Because of the negligible effect of SiO_2 on the grain boundary (ICP: SiO_2 wt% < 50 ppm), the grain boundary resistance is created only by space charge layer [31]. That is, the accumulation of acceptor cations at the grain boundaries, as a result of elastic strain and Coulomb interactions, leads to the oxygen vacancy depletion in the vicinity of the grain boundary and subsequently the reduction of the grain boundary conductivity. Therefore, more doping elements segregating to grain boundaries can result in lower grain boundary conductivity at the same doping level. In order to analyze the segregation, XPS spectra are introduced. The sample of $Ce_{0.9}(Sm_{0.5}Nd_{0.5})_{0.1}O_{1.95}$ is taken as an example. Fig. 6(a) shows that grain boundaries of the sample contains not only Ce, Nd, Sm and O elements, but also some C elements. The XPS peak for C1s at Eb = 285 eV is ascribed to the hydrocarbon from the XPS instrument itself. Fig. 6(b)–(d) display the high-resolution XPS spectra of Ce, Sm and Nd at grain boundaries, which can be used to calculate the elemental composition (at.%) of grain boundaries. The results are listed in Table 3. The samples of $Ce_{0.9}Nd_{0.1}O_{1.95}$ and $Ce_{0.9}Sm_{0.1}O_{1.95}$ are analyzed with the same method. It can be seen from Table 3 that the values of doping element/Ce are larger at grain boundaries than in the grain, clarifying the segregation of doping ion at the grain boundaries. Especially, the specimen of $Ce_{0.9}Sm_{0.1}O_{1.95}$ exhibits the highest value of 24 at.%. This indicates the amount of Sm^{3+} segregating to the grain boundary is much more than that of Nd^{3+}, which can be used to explain that

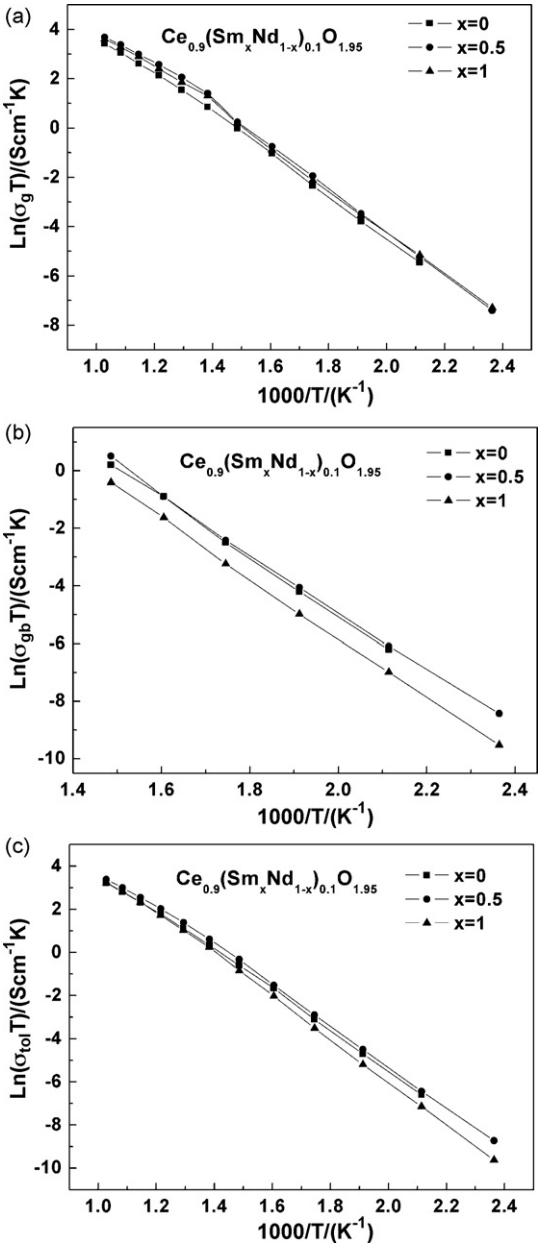

Fig. 4. Grain (a), grain boundary (b) and total electrical conductivity (c) of $Ce_{0.9}(Sm_xNd_{1-x})_{0.1}O_{1.95}$ sintered at 1400 °C for 4 h with $x = 0$, 0.5 and 1.

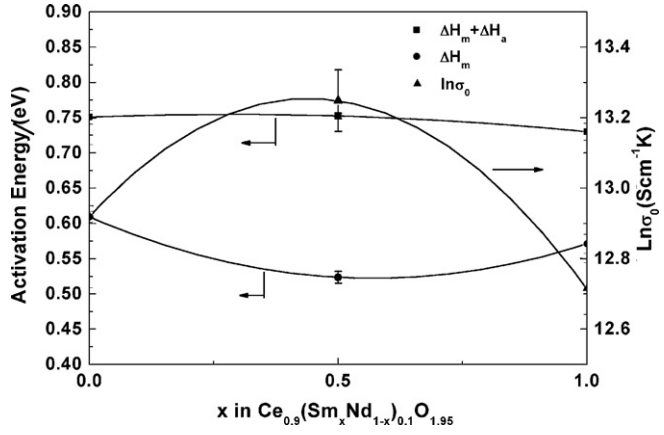

Fig. 5. Activation energies and $\ln\sigma_0$ of the grain for the series of $Ce_{0.9}(Sm_xNd_{1-x})_{0.1}O_{1.95}$.

Table 3
Atomic percentage of doping element/Ce in the grain and grain boundary, and Sm/Nd in the grain boundary for different compositions.

Composition	Doping element/Ce (at.%, grain)	Doping element/Ce (at.%, grain boundary)	Sm/Nd (at.%, grain boundary)
$Ce_{0.9}Sm_{0.1}O_{1.95}$	11	24	–
$Ce_{0.9}(Sm_{0.5}Nd_{0.5})_{0.1}O_{1.95}$	11	13	170
$Ce_{0.9}Nd_{0.1}O_{1.95}$	11	13	–

$Ce_{0.9}Sm_{0.1}O_{1.95}$ possesses lower grain boundary conductivity than $Ce_{0.9}Nd_{0.1}O_{1.95}$ (Fig. 4(b)). However, for $Ce_{0.9}(Sm_{0.5}Nd_{0.5})_{0.1}O_{1.95}$, the segregation is suppressed and the value of doping element/Ce is close to that of $Ce_{0.9}Nd_{0.1}O_{1.95}$, which corresponds to the similar grain boundary conductivity, as shown in Fig. 4(b). And furthermore, seen in Table 3, for $Ce_{0.9}(Sm_{0.5}Nd_{0.5})_{0.1}O_{1.95}$, the value of Sm/Nd is about 170 at.%, showing that the segregation of Sm^{3+} is prior to that of Nd^{3+} to the grain boundaries. As mentioned above, the differences in grain boundary behavior for samples correspond to differences in the trivalent dopant segregation. The amount and order of segregation under the same sintering condition is reported to be perhaps relative to bond dissociation enthalpy values of Ln–O (Ln = rear earth elements) [28], which are $\Delta H_{bdiss} = 619$ and 703 kJ mol^{-1} for bonds Sm–O and Nd–O, respectively [32]. Low bond dissociation enthalpy would contribute to lower the excess energy at grain boundaries, corresponding to lower grain boundary conductivity, which is consistent with the results in our case. Therefore, not only does ceria co-doped with Sm and Nd increase the grain conductivity but also improve the grain boundary conductivity. $Ce_{0.9}(Sm_{0.5}Nd_{0.5})_{0.1}O_{1.95}$ have the highest total conductivity with the value of 1.0×10^{-2} S cm^{-1} at 550 °C. In our previous study [13], in the series of $Ce_{0.8}(Sm_xNd_{1-x})_{0.2}O_{1.9}$, the total conductivity exhibits the maximum value with $x = 0.5$, which is consistence with that of the series of $Ce_{0.9}(Sm_xNd_{1-x})_{0.1}O_{1.95}$.

For ceria doped with Sm [16,17], Nd [18,19], Gd [20], Y [15] and so on, the total conductivity is relative to doping content. In our work, the ratio of Sm to Nd is fixed at 1:1, and the total amount of dopants was changed in order to search for an appropriate one with higher conductivity. Fig. 7 shows grain, grain boundary and total conductivity of the series of $Ce_{1-x}(Sm_{0.5}Nd_{0.5})_xO_\delta$ with $x = 0.05$, 0.10, 0.15, and 0.20. As shown in Fig. 7(a), the grain conductivity of the samples increases with the amount of dopant up to $x = 0.10$, followed by a decrease, and the composition of $x = 0.10$ turns up to be a turning point with the maximum value of 1.6×10^{-2} S cm^{-1} measured at 550 °C. Besides, the curvature on the Arrhenius plot for the compositions of $Ce_{1-x}(Sm_{0.5}Nd_{0.5})_xO_\delta$ can be observed, which has previously been found for numerous ceria-based solid solutions, including $Ce_{1-x}Gd_xO_\delta$, $Ce_{1-x}Sm_xO_\delta$, $Ce_{1-x}Nd_xO_\delta$, and $Ce_{1-x}Y_xO_\delta$ [15–20]. Seen from Fig. 7(a), the transition occurs among 400–500 °C. The grain activation energies of $Ce_{1-x}(Sm_{0.5}Nd_{0.5})_xO_\delta$ for different temperature ranges are displayed in Fig. 8. It can be seen that when $x = 0.05$, the transition point is not obvious. With increasing the amount of dopants, the activation energies at higher and lower temperature ranges both increases, but the association enthalpy exhibits the maximum value at $x = 0.10$. This trend is coincident with that of $Ce_{1-x}Nd_xO_\delta$ reported by Stephens and Kilner [18]. However, for $Ce_{1-x}Sm_xO_\delta$, the association enthalpy is larger at $x = 0.30$ or 0.4 [16,17]. Two reverse factors may lead to the association enthalpy with maximum value at some concentration. On the one hand, with increasing the amount of dopants, dimmers ($[M'_{Ce}][V_{\ddot{O}}]$), trimers ($[V_{\ddot{O}}][M'_{Ce}][V_{\ddot{O}}]$) and higher order clusters may exist which may possess particularly high binding energies, resulting in the improvement of the association enthalpy. The order clusters can disassociate at higher temperature. On the other hand, in the heavily doped samples, the local ordering (microdomain) of oxygen vacancies may happen as

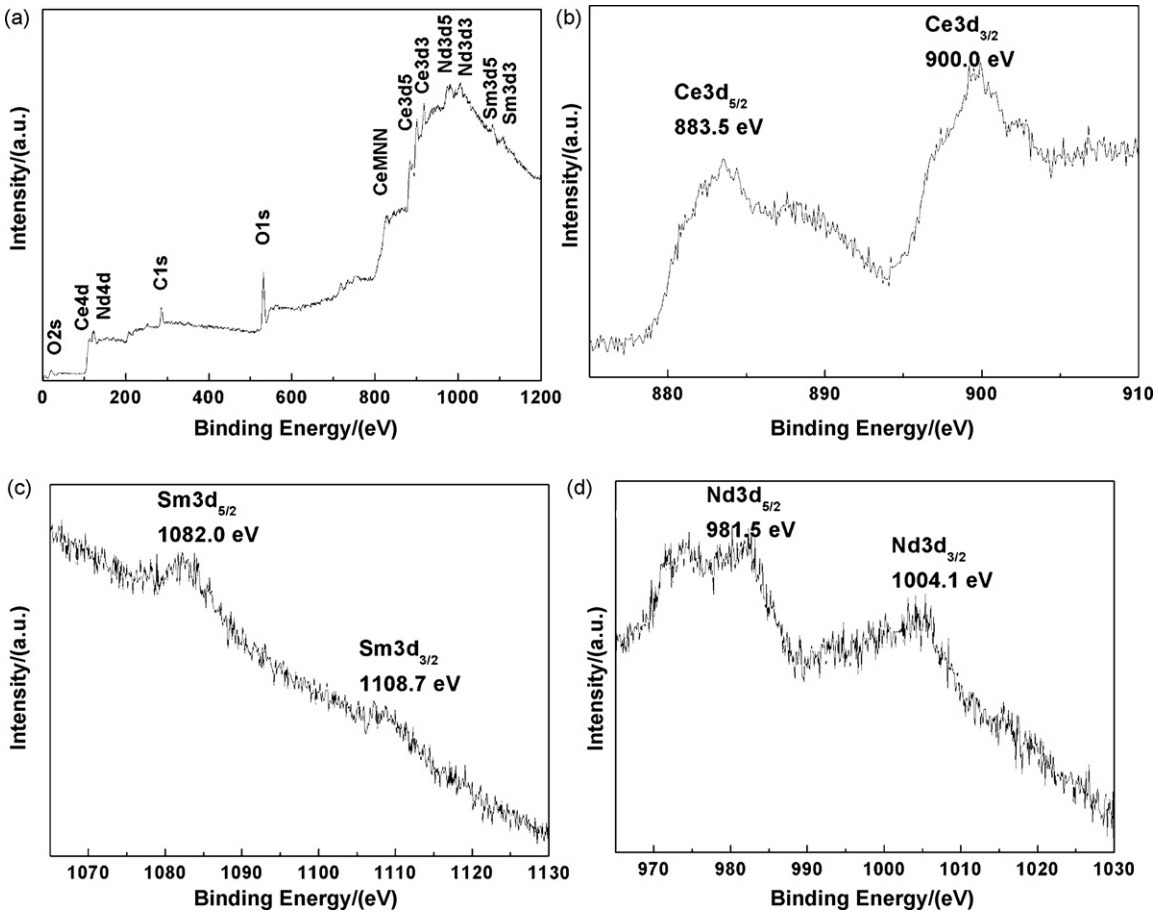

Fig. 6. XPS spectra of $Ce_{0.9}(Sm_{0.5}Nd_{0.5})_{0.1}O_{1.95}$: full spectrum of the sample (a); Ce 3d spectrum (b); Sm 3d spectrum (c); Nd 3d spectrum (d).

precursors to the eventual precipitation of regions of C-type rare earth oxides, and cannot be disassociated at higher temperatures. Therefore, the increase of the activation energies with increasing the doping contents in lower temperature ranges is relative to the formation of both order clusters and local ordering. However, the increase of the activation energies in higher temperature ranges is only relevant to an increase in the local ordering, which is consistent with the observations of Ou et al. [33]. As investigated by them, this local ordering cannot be identified by XRD, and comparative studies of EELS and SAED have clearly shown an increase in the local ordering is observed with increasing the doping concentration and decreasing the doping ion radius from Sm^{3+} to Yb^{3+}, which has also been indirectly confirmed by aging behavior of doped ceria reported by Zhang et al. [34]. Therefore, due to the lager ion radius of Nd^{3+} than that of Sm^{3+}, it can be presumed that the local ordering of oxygen vacancies could occur more easily in Nd-doped ceria than in Sm-doped ceria. Due to the existence of Nd^{3+}, the trend of $Ce_{1-x}(Sm_{0.5}Nd_{0.5})_xO_\delta$ about the association enthalpy is similar to that of $Ce_{1-x}Nd_xO_\delta$, as shown in Fig. 8.

Fig. 7(b) shows the grain boundary conductivity of $Ce_{1-x}(Sm_{0.5}Nd_{0.5})_xO_\delta$. As listed in Table 1, the relative density of every composition is almost the same, so the grain boundary dominantly depends on the composition. With increasing the concentration of dopants, the grain boundary conductivity increases first, and then decreases. The composition at $x = 0.10$ possesses the highest grain boundary conductivity. The grain boundary activation energies are estimated from Fig. 7(b) according to Eq. (1) and shown in Fig. 9. The composition of $Ce_{1-x}(Sm_{0.5}Nd_{0.5})_xO_\delta$ at $x = 0.10$ has the lowest grain boundary activation energy. As is similar to the case of grain conductivity, the decrease of grain boundary activation energy is perhaps due to the presence of attractive interactions between dopant cations and oxygen vacancies in the space charge layer, due to the increase in dopant concentration leading to an increase in the number of percolation paths. And the increase of grain boundary activation energy with increasing content is also relative to the ordering of oxygen vacancies in space charge layers. For comparison, the grain boundary activation energies for $Ce_{1-x}Sm_xO_\delta$ [17] and $Ce_{1-x}Nd_xO_\delta$ [19] are both cited, and also shown in Fig. 9. From Fig. 9, it can be observed that the trend of $Ce_{1-x}(Sm_{0.5}Nd_{0.5})_xO_\delta$ is similar to that of $Ce_{1-x}Nd_xO_\delta$, with the lowest value at the same composition $x = 0.10$. But for $Ce_{1-x}Sm_xO_\delta$, the grain boundary activation energy has the lowest value at $x = 0.2$. The phenomenon can be explained as follows: for $Ce_{1-x}(Sm_{0.5}Nd_{0.5})_xO_\delta$, the segregation amount of Sm^{3+} is more than that of Nd^{3+} to the grain boundary, as measured by XPS (Table 3), leading to much more Nd^{3+} than Sm^{3+} in the space charge layer regions and similar space charge layer region, and hence similar electrical property of grain boundaries to that of $Ce_{1-x}Nd_xO_\delta$.

Fig. 7(c) shows the total conductivity of $Ce_{1-x}(Sm_{0.5}Nd_{0.5})_xO_\delta$. Due to the two effects of grain and grain boundary, the composition at $x = 0.10$ exhibits the highest total conductivity. As mentioned in the introduction, up to now, $Ce_{0.9}Gd_{0.1}O_{1.95}$ and $Ce_{0.8}Sm_{0.2}O_{1.9}$ are reported to have higher total conductivity [1–3]. For comparison, the $Ce_{0.9}Gd_{0.1}O_{1.95}$ and $Ce_{0.8}Sm_{0.2}O_{1.9}$ powers were also synthesized by citric acid–nitrate low-temperature combustion process, and then sintered at 1400 °C for 4 h. Compared with them, $Ce_{0.9}(Sm_{0.5}Nd_{0.5})_{0.1}O_{1.95}$ possesses higher conductivity, which is due to the lower activation energy, as shown in Figs. 7(c) and 8, and consistent with the calculation results of Andersson et al. [12].

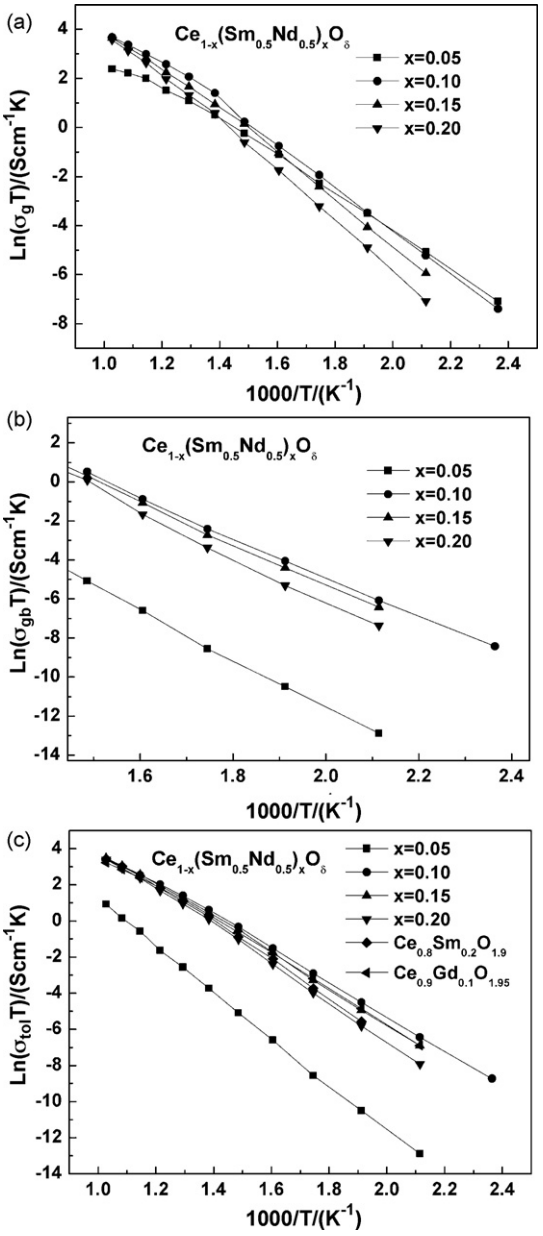

Fig. 7. Grain (a), grain boundary (b) and total conductivity (c) of the series of $Ce_{1-x}(Sm_{0.5}Nd_{0.5})_xO_\delta$ with $x = 0.05$, 0.10, 0.15, and 0.20.

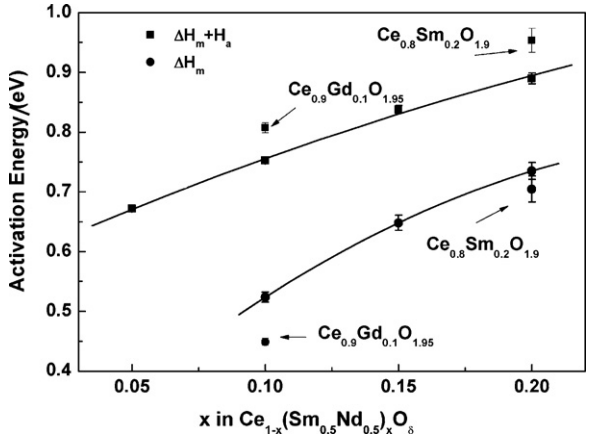

Fig. 8. Activation energies of the grain as a function of dopant concentration for $Ce_{1-x}(Sm_{0.5}Nd_{0.5})_xO_\delta$.

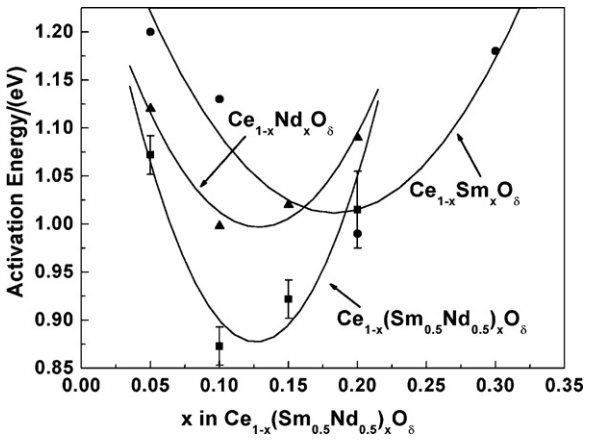

Fig. 9. Activation energies of the grain boundary as a function of dopant concentration for $Ce_{1-x}(Sm_{0.5}Nd_{0.5})_xO_\delta$.

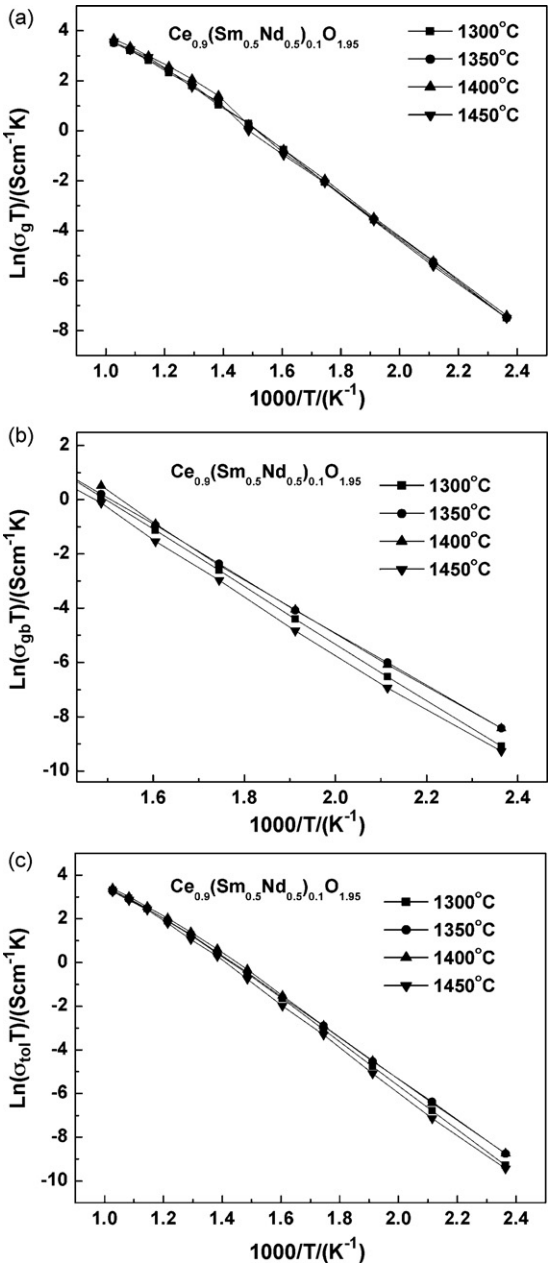

Fig. 10. Grain (a), grain boundary (b) and total conductivity (c) of $Ce_{0.9}(Sm_{0.5}Nd_{0.5})_{0.1}O_{1.95}$ sintered at different temperatures from 1300 °C to1450 °C.

By the discussion above, $Ce_{0.9}(Sm_{0.5}Nd_{0.5})_{0.1}O_{1.95}$ has the highest conductivity for the series of $Ce_{1-x}(Sm_{0.5}Nd_{0.5})_xO_\delta$. In order to optimize the conductivity, a suitable sintering scheme is needed. As displayed in Fig. 10(a), the sintering temperature has negligible effect on the grain conductivity. However, it can be observed from Fig. 10(b) that the samples sintered at 1350 °C and 1400 °C posses higher grain boundary conductivity. In this study, as mentioned above, the grain boundary resistance is proposed mostly owing to the segregation of acceptor cations to the grain boundary. Moreover, the diffusion process of doping ions is relative to sintering temperature. Although high sintering temperature can result in the improvement of the density and the reduction of high-resistivity grain boundary, as listed in Table 2, simultaneously it might lead to the well developed space charge layer regions. Owing to the two antagonist influencing factors, the appropriate sintering temperature ranges (1350–1400 °C) with the maximum grain boundary conductivity value present, as shown in Fig. 10(b). For the same reason, the samples sintered at 1350 and 1400 °C exhibit higher total conductivity ascribed to the constant grain conductivity, which agrees with the tendency of grain boundary conductivity, as shown in Fig. 10(c).

4. Conclusions

In summary, ceria co-doped with Sm and Nd powders were successfully prepared by citric acid–nitrate low-temperature combustion process. The effects of co-doping, doping content and sintering conditions on grain and grain boundary conductivity for ceria co-doped with Sm^{3+} and Nd^{3+} were investigated in detail. It was found, for the series of $Ce_{0.9}(Sm_xNd_{1-x})_{0.1}O_{1.95}$ (x = 0, 0.5, 1), the composition at x = 0.5 exhibited higher grain and grain boundary conductivity. $Ce_{0.9}Sm_{0.1}O_{1.95}$ showed significantly lower grain boundary conductivity due to serious segregation of Sm^{3+} to the grain boundary measured by XPS. For $Ce_{1-x}(Sm_{0.5}Nd_{0.5})_xO_\delta$ (x = 0.05, 0.10, 0.15, 0.20) sintered under the same condition, the composition at x = 0.10 also exhibited higher grain and grain boundary conductivity. Moreover, when the composition was x = 0.10, the grain association enthalpy was highest, and the grain boundary activation energy was lowest, which were both consistent with those of $Ce_{1-x}Nd_xO_\delta$, but different from those of $Ce_{1-x}Sm_xO_\delta$. This phenomenon can be explained as follows: the local ordering of oxygen vacancies maybe happens more easily in Nd-doped ceria than in Sm-doped ceria; the amount of Sm^{3+} is more than that of Nd^{3+} segregating to grain boundaries in ceria co-doped with Sm^{3+} and Nd^{3+}, which was confirmed by XPS. In addition, for the sample of $Ce_{0.9}(Sm_{0.5}Nd_{0.5})_{0.1}O_{1.95}$, the sintering temperature had negligible effect on grain conductivity, and the sample sintered at 1350–1400 °C showed higher total conductivity with the value of 1.0×10^{-2} S cm^{-1} at 550 °C resulting from higher grain boundary conductivity, which was higher than that of $Ce_{0.9}Gd_{0.1}O_{1.95}$ and $Ce_{0.8}Sm_{0.2}O_{1.9}$.

Acknowledgement

This research was supported by Toyota Motor Corp.

References

[1] V.V. Kharton, F.M.B. Marques, A. Atkinson, Solid State Ionics 174 (2004) 135–149.
[2] J.B. Goodenough, Annu. Rev. Mater. Res. 33 (2003) 91–128.
[3] L. Anna, J. Skinner Stephen, J. Mater. Chem. 16 (31) (2006) 3161–3170.
[4] S. Banerjee, P.S. Devi, D. Topwal, S. Mandal, K. Menon, Adv. Funct. Mater. 17 (2007) 2847–2854.
[5] S. Omar, E.D. Wachsman, J.C. Nino, Solid State Ionics 177 (2006) 3199–3208.
[6] M. Dudek, W. Bogusz, L. Zych, B. Trybalska, Solid State Ionics 179 (2008) 164–167.
[7] S. Omar, E.D. Wachsman, J.C. Nino, Appl. Phys. Lett. 91 (2007) 144106–144108.
[8] H. Xu, H. Yan, Z. Chen, J. Power Sources 163 (2006) 409–414.
[9] D. Pérez-Coll, P. Núñez, J.R. Frade, J.C.C. Abrantes, Electrochim. Acta 48 (2003) 1551–1557.
[10] J.A. Kilner, R.J. Brook, Solid State Ionics 6 (1982) 237.
[11] D.-J. Kim, J. Am. Ceram. Soc. 72 (1989) 1415–1421.
[12] D.A. Andersson, S.I. Simak, N.V. Skorodumova, L.A. Abrikosov, B. Johansson, PNAS 103 (10) (2006) 3518–3521.
[13] Y.Y. Liu, B. Li, X. Wei, W. Pan, J. Am. Ceram. Soc. 91 (12) (2008) 3926–3930.
[14] S. Omar, E.D. Wachsman, J.C. Nino, Solid State Ionics 178 (37–38) (2008) 1890–1897.
[15] T. Chunyan, C. Siuwai, Solid State Ionics 134 (2000) 89–102.
[16] Z. Zhan, T.-L. Wen, H. Tu, Z.-Y. Lu, J. Electrochem. Soc. 148 (5) (2001) A427–A432.
[17] D. Pérez-Coll, P. Núñez, J.R. Frade, J. Electrochem. Soc. 153 (3) (2006) A478–A483.
[18] I.E.L. Stephens, J.A. Kilner, Solid State Ionics 177 (2006) 669–676.
[19] J.X. Zhu, D.F. Zhou, S.R. Guo, J.F. Hao, X.Q. Cao, J. Meng, J. Power Sources 174 (2007) 114–123.
[20] D. Pérez-Coll, P. Núñez, J.C. Ruiz-Morales, J. Peña-Martínez, J.R. Frade, Solid State Ionics 176 (2005) 2799–2805.
[21] X. Sha, Z. Lu, X. Huang, J. Miao, Z. Liu, X. Xin, Y. Zhang, W. Su, J. Alloys Compd. 433 (2007) 274–278.
[22] B. Li, X. Wei, W. Pan, J. Power Sources 183 (2008) 498–505.
[23] H. Li, C. Xia, M. Zhu, Z. Zhou, G. Meng, Acta Mater. 54 (2006) 721–727.
[24] D.R. Qu, T. Mori, F. Ye, M. Takahashi, J. Zou, J. Drennan, Acta Mater. 54 (2006) 3737–3746.
[25] G.S.A.M. Theunissen, A.J.A. Winnubst, A.J. Burggraaf, J. Mater. Sci. 27 (1992) 5057–5066.
[26] M.I. Mendelson, J. Am. Ceram. Soc. 52 (1969) 443–446.
[27] S.J. Hong, Virkar S A.V., J. Am. Ceram. Soc. 78 (2) (1995) 433–439.
[28] D. Pérez-Coll, D. Marrero-Lopez, P. Núñez, S. Piñol, J.R. Frade, Electrochim. Acta 51 (2006) 6463–6469.
[29] B.C.H. Steele, Solid State Ionics 129 (2000) 95–110.
[30] H. Yamamura, E. Katoh, M. Ichikawa, K. Kakinuma, T. Mori, H. Haneda, Electrochemistry 68 (6) (2000) 455–459.
[31] X. Guo, R. Waser, Prog. Mater. Sci. 51 (2006) 151–210.
[32] J.A. Dean (Ed.), Lange's Handbook of Chemistry, McGraw-Hill, 1979.
[33] D.R. Ou, T. Mori, F. Ye, J. Zou, G. Auchterlonie, J. Drennan, Phys. Rev. B 77 (2008) 024108–024115.
[34] T.S. Zhnag, J. Ma, L.B. Kong, S.H. Chan, J.A. Kilner, Solid State Ionics 170 (2004) 209–217.